**Journal of Sciences, Islamic Republic of Iran 24(2): 113-122 (2013)** http://jsciences.ut.ac.ir
University of Tehran, ISSN 1016-1104

# Compound Action Potential of Isolated Spinal Cord: A Biophysical Analysis to Address Activity of Individual Fibers Following Contusion Injury

I. Rad,[1] K. Khodayari,[1] S. Kouhzaei,[1] and H. Mobasheri[1,2,*]

[1]*Laboratory of Membrane Biophysics, Institute of Biochemistry and Biophysics, University of Tehran, Tehran, Islamic Republic of Iran*
[2]*Biomaterials Research Centre (BRC), University of Tehran, Tehran, Islamic Republic of Iran*

Received: 24 February 2013 / Revised: 10 June 2013 / Accepted: 18 June 2013

## Abstract

Compound action potential (CAP) of spinal cord represents valuable properties of neural fibers including excitability, rate of myelination and membrane integrity. These properties are measured using amplitude, latency and area under curve of CAPs recorded from spinal cord. Here, the isolated spinal cord was set in a double sucrose gap (DSG) chamber and its response to intracellular stimulation was recorded as a CAP signal. Lateral and Dorsal-ventral mechanical presures were then applied on whole spinal cord (WSC) and spinal cord strips (SCS) of isolated spinal cord to mimic spinal cord injury (SCI). In order to identify a representative pattern of CAP applicable in SCI, the recoded CAPs were evaluated, averaged and fitted using Matlab curve fitting toolbox. The results showed a significant decline in the amplitude and conduction velocity (CV) of CAPs caused by SCI in WSC and SCS preparations. This phenomenon was more significant in less myelinated fibers than highly myelinated motoneurons (MNs) and was identified as a decline in the fitted model level. Differential CAPs of WSC and SCS represented mono and biphasic curves that were fitted to Gaussian model levels of "G4" and "G6", respectively. However, the CAP of injured WSC and SCS preparations fitted to Gaussian model level three "G3". Based on the comparative study of WSC and SCS preparations the MN pathways can be traced by recorded CAPs. The current approach can be applied in the identification and evaluation of spinal cord function for experimental and clinical purposes.

**Keywords:** Biophysics; Compound action potential (CAP); Gaussian model; Spinal cord Injury (SCI); Double sucrose gap (DSG)

## Introduction

Spinal cord white matter (WM) of rat has an extensive application in basic and translational medicine researches. Compound action potential (CAP) recording is known as a real-time tool for characterizing

* Corresponding author, Tel.: +98(21)66956982, Fax: +98(21)66956982, E-mail: h.mobasheri@ibb.ut.ac.ir

physiological properties of WM in multi-axonal populations. Unlike single fiber electrophysiological recordings, CAPs are not critically dependent on stimulation intensity [1]. This advantage of CAP facilitates reproducible recordings. Immobilized stimulating and recording electrodes are used to reinforce this advantage in ex-vivo models like double sucrose gap (DSG). DSG has been used as an intra-axonal CAP recording tool though characteristics of recorded CAP and its corresponding pathways were less discussed [2].The shunting effect of extracellular fluid caused in CAP recording is minimized through the application of isotonic sucrose solution in the DSG model where electric current is exclusively conducted through spinal cord pathways. There is also an increment in the efficiency of stimulation implemented by lowering stimulus intensity. This improves the CAP recording due to removal of stimulus artifact that meddles with recorded CAPs [3]. Since there is a need for several trials to generate a reproducible CAP, finding a pattern that describes recorded CAPs would eliminate number of trials [4].To fulfil this aim, the averaged recorded CAPs were fitted to parametric models to introduce an effective improvement in the monitoring process.

The WM has been extensively used in experimentally induced demyelination or hypoxic/ ischemic injury studies [5]. Despite the heterogeneity of neural populations, rodent recorded CAPs from WM represented a typical peak shape [5]. The increased stimulation intensity is not followed by the increase in amplitude of recorded CAPs when all fibers are activated. In some circumstances, WM CAP decay is prolonged by a slower conducting peak that is known as "C-wave" [2]. It was also shown that two components appearing in CAPs are generated mostly by myelinated axons. These axons possess conduction velocities (CVs) of more than 5 m/s in rat spinal cord WM. There is a unimodal histogram that represents axon diameters in WM in the range of 1-6 μm [5].

Descending signals travel through the "pyramids" of the medulla to their targets and are called "pyramidal pathway". It makes the MNs efferent conduction route in combination with extrapyramidal pathway. Extrapyramidal pathway is concerned with the rapid reflexes and postural control rather discrete voluntary movements that are conducted through the pyramidal pathway. Extrapyramidal pathways recruit highly myelinated fibers to achieve their demanded CV that is required for their function [6].

The Remak bundles accompanied with the distal peripheral nerves are associated with afferent axons due to functional inferences. Thus, the Remak bundles are considered as the axon assembly of C-fibers in rat PNS. They exit from the dorsal root ganglion (DRG) at L5 in Lumbar area that contains 56% of spinal cord unmyelinated axons. [7]. Poorly myelinated fibers (e.g. C-fibers) are known to be demonstrated as C-wave in spinal cord recorded CAPs. The C wave conduction velocity, dependence on stimulus intensity and strength-duration properties of recorded CAP are similar to unmyelinated fibers.

Neuromodulators change membrane potential in unmyelinated peripheral axons [8]. Motoneurons (MNs) responsiveness to stimulants and their excitability is also regulated by neuromodulators. "C boutons" originate from lateral interneurons of the central canal. Abundant cholinergic ''C boutons'' around MN somata are known as neuromodulators that activate m2 receptors through MNs excitability regulation. Endogenous cholinergic inputs raise MNs excitability in isolated spinal cord preparations [9].

In this study, descending volleys applied on whole spinal cord (WSC) and spinal cords strips (SCS) and were recorded in ex-vivo condition using double sucrose gap (DSG) chamber. Abrupt mechanical injury was simulated through the application of Aneurism clip to impose mechanical localized forces on WSC and SCS preparations. Different fitting models were applied to analyse the recorded CAPs from normal and damaged WSC and SCS preparations to find the best deterministic and comprehensive description of their corresponding CAPs. The fitted CAPs were used to address the corresponding damaged fibers in the spinal cord.

## Materials and Methods

### *Spinal Cord Injury Model*

*Anaesthesia Condition*

Adult male Wistar rats (250-300g) were anaesthetized with intraperitoneal injections of Ketamine hydrochloride (80 mg/Kg) and Xylazine (12 mg/Kg) from Alfasan-Holland.

### *Spinal Cord Isolation*

A total of 30 adult male Wistar rats (weight 250–300g) were deeply anaesthetized as mentioned above. To remove blood and lower the cord temperature, transcardial perfusion was performed using 200 ml oxygenated cold Krebs solution (NaCl 124mM; KCl 2mM; KH2PO4 1.2mM; MgSO4 1.3mM; CaCl2 2mM; dextrose 20mM; sodium ascorbate 10mM; NaHCO3

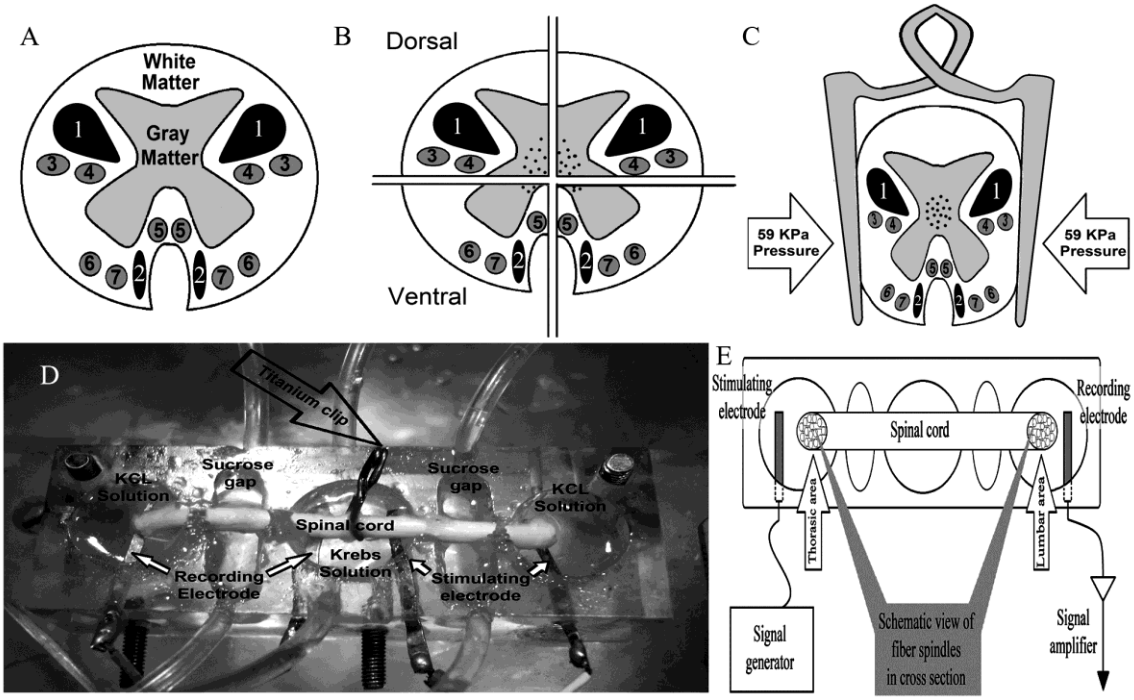


**Figure 1**. Neural tracts of isolated spinal cord. (A) Schematic cross section of spinal cord. Lateral corticospinal (LCS) and anterior corticospinal (ACS) tracts, are shown by numbers 1 and 2 respectively. Rubrospinal, reticulospinal and vestibulospinal tracts are marked by numbers 3, 4 and 7 respectively. There are also two olivospinal tracts that are marked as 5 and 6. Pyramidal and extrapyramidal pathways are represented in dark and pale, respectively. (B) Transected strips for DSG. Black spots of grey matter that are positioned around central canal are representatives of "C-boutons" (C) Schematic cross section of introduced clip in an *ex vivo* abrupt compression. (D) isolated whole spinal cord (WSC) in DSG chamber (*Ex vivo* model). (E) Schematic view of double sucrose gap (DSG) stimulation and record system.

26mM, from Sigma). Following rapid excision of the spine, a complete laminectomy was performed to expose the spinal cord. The whole spinal cord (WSC) was then removed from the vertebrae and stabilized by incubation in oxygenated Krebs solution, bubbled with an $O_2/CO_2$ (95/5 v/v) gas mixture, for an hour at room temperature. The isolated spinal cord was then immersed in oxygenated Krebs buffer and dissected to dorsal or ventral longitudinal quadrants strips. The whole procedure was conducted based on the preparation method reported by Shi et al [10]. Every effort was made to minimize the suffering and the number of the animals used. The experimental protocols have been reviewed and approved by the Faculty of Veterinary Medicine, University of Tehran and Society for Prevention of Cruelty to Animals (SPCA).

### *Ex-Vivo Recording*

The isolated spinal cord sealed in the double sucrose chamber (DSC) initially introduced by Shi et al [14]. The double sucrose gap chamber constructed of PlexiglassTM. It consists of three large compartments (each with a volume of 2ml) separated by two narrow reservoirs (each with a volume of 1ml). The middle compartment that represented extracellular medium was filled with oxygenated modified Krebs solution and the other two compartments were filled with isotonic potassium chloride (120 mM). The separating compartments were filled with non-conductive isotonic sucrose to separate the intracellular medium of the spinal cord fibers from the extracellular side, electrically (Fig. 1-D). Complete isolation of the compartments was achieved by silicone grease sealing. Different Peristaltic pumps continuously circulated the oxygenated Krebs and isotonic sucrose solutions. Stimulation of the spinal cord at the proximal end produced CAP signals that were recorded by silver/silver chloride electrodes positioned at the distal end and the middle reservoir was grounded (Fig. 1-E). All the WSC and SCS preparations received maximum stimulus intensity to recruit evoked potential of all fibers in recorded CAP (1-3 V, 0.1 ms peak to peak). The distance between stimulating and recording electrode was 40-45 mm.

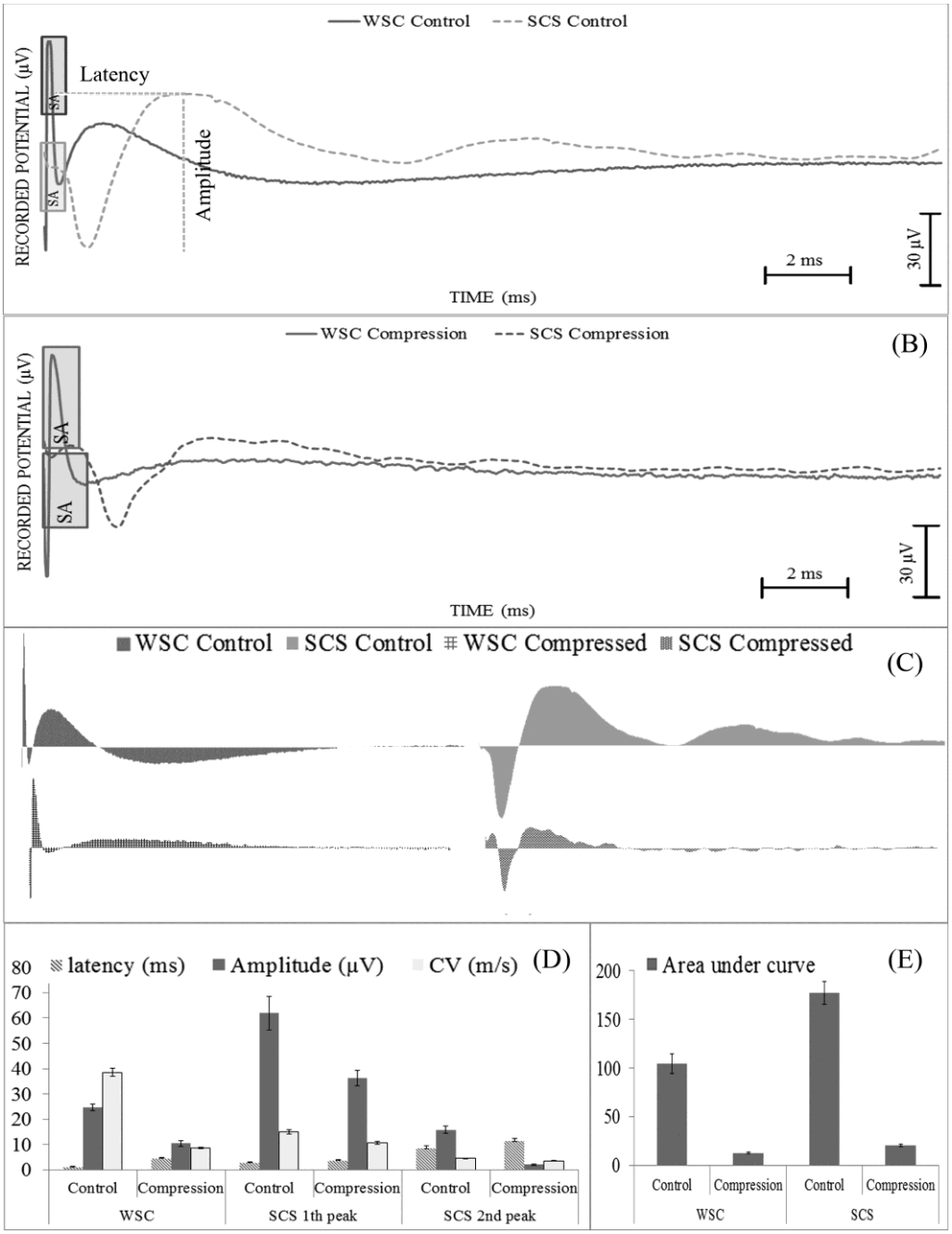


**Figure 2**. Averaged CAPs of WSC and SCS in intact and injured states. (A) Recorded CAP, latency and its amplitude in non-injured whole spinal cord (WSC) and spinal cord strip (SCS). "SA" stands for stimulation artifact. (B) Recorded CAP after abrupt compression in WSC and SCS. (C) Area under curve of WSC and SCS CAPs. (D, E) Calculated latency, amplitude, CV and area under curve of averaged CAPs are shown, respectively.

### *CAP Characteristics*

The isolated spinal cord was sealed in the chamber and its activity was recorded before compression at 37°C. The recordings were repeated ten times and the averaged values were used for statistical analysis. To quantify the CAP signals, the area under CAP's peaks, their CV, latency and amplitudes were measured in different groups (Fig. 2). The area under CAP curve demonstrates overall conduction of recruited fibers

while CV reveals conduction speed of definite tract fibers in meter per second. The appropriate time at which individual CAP peaks appeared was considered as latency. Amplitude strength of recorded peaks in CAP addressed the excitability of corresponding evoked fibers.

$$CV = \frac{\text{Distance between stimulating and recording electrodes}(\text{mm})}{\text{latency}(\text{ms})}$$

**(Equation 1)**

### *Statistical Analysis*

The amplitude, latency and area under peak of CAPs were averaged, analyzed and expressed as mean ± SD. The results were statistically evaluated using Student's t-tests, and differences were considered significant if $P<0.05$.

### *Parametric Fitting Models*

The averaged recorded CAPs shared two deterministic and random components. The fitting model simulated the deterministic component and the random components were described as associated errors. The valley appeared before the first peak was taken into account to determine the peak latency with respect to stimulus artifact. The stimulus artifacts were ignored in all fitted curves.

### *Parametric Models*

Fourier series, Sum of Sines, Polynomial, and Gaussian models were used to describe CAP properties. The Fourier series is a sum of sine and cosine functions that are used to describe a periodic signal. Taking this approach, the frequencies of different peaks appearing in CAPs were analysed accordingly. The sum of sines model that is used for fitting periodic functions was applied to identify repeatability of the individual peaks.

Polynomial models describe the shape of peaks using terms of different powers. Feeding the model by our experimental data, the ascending and descending trend of each peak was represented by the corresponding equation. The Gaussian model was applied to study the amplitude, time base location and duration of all peaks forming the CAP and is represented by the following equation:

$$y = \sum_{i=1}^{n} a_i e^{\left[-\left(\frac{x-b_i}{c_i}\right)^2\right]} \qquad \textbf{(Equation 2)}$$

Where a is the amplitude, b is the centroid (location), c is related to the peak width and n is the number of peaks to fit ($1 \le n \le 8$).

### *Evaluation of Statistical Approaches*

After data fitting, goodness of fitting was evaluated for each model. The appropriateness of visual examination for fitted curves was the first step followed by three more steps including; i) evaluation of residuals inclusiveness, ii) statistical terms consideration and iii) visual estimation of prediction bounds. The summary of evaluating the goodness of fitting is shown in Figure 3 (Step 1-3).

The residuals from a fitted model were defined as the differences between the response data and the fit at each predictor value.

The statistical parameters including: sum of squares due to error (SSE) adjusted R-square and root mean squared error (RMSE) and prediction bounds (confidence) were applied for further validation of the approaches taken. In a proper fit, adjusted R-square amount was very close to one while the RMSE and SSE are close to zero.

Thus, the total deviation of the response values, successfulness of the fit, variation of the data (standard error) and fitted curve deviation, were measured by statistical parameters [11].

Since removal of the artifacts and the convolution with the Gaussian template generates a clean CAP signal, exclusion mode was carried out to gain a suitable goodness of fitting. The trust-region algorithm was chosen for fitting model without using robust item. This limit was elected according to normal ±50 mv. According to averaged experimental measurements, CAP recurrence frequency was considered as 33.3 Hz.

The analysis demonstrated that a minimum of 10 trials was sufficient to obtain an acceptable fidelity in the detection of the time-frequency domains. The peak latency was measured from the onset of the stimulus to the peak of each wave. The amplitude was measured from the peak of one polarity to the next peak of the opposite polarity [12]. The averaged representative traces of CAPs are shown in Figure 2 (A, B).

Amplitude and latency deviation revealed that the location of peaks does not deviate by more than 25% from the baseline and the peak-to-peak amplitude does not deviate by more than 10%. The area under averaged CAPs was calculated by the Simpson method (Fig. 2-C, D, E) [13, 14].

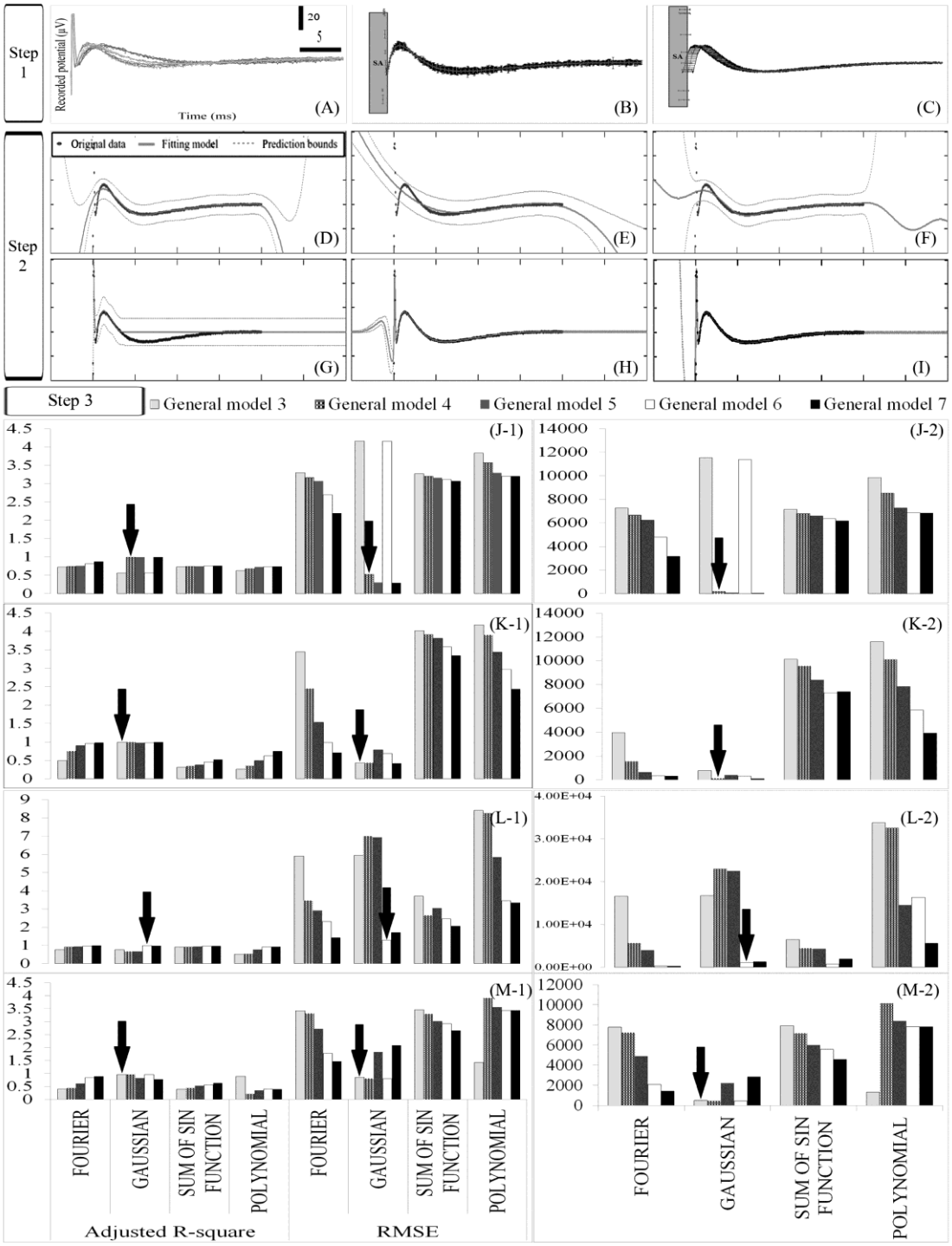


**Figure 3**. Fitting method summary. Step 1; (A) Recorded CAPs at different stimulus intensities. (B, C) Averaged data from optimized recording. Error bars represent the standard deviation of amplitude and latency, respectively. "SA" stands for stimulation artifact. Step 2; (D) Fitting of the results using Fourier model 4. (E) Fitting of the results using Polynomial model 4. (F) Fitting of the results using Sum of sin functions model 4. (G-I) Fitting of the results using Gaussian models of 3-5, respectively. Step 3; Column 1 and 2 represents adjusted $R^2$, root mean squared error (RMSE) of fitting models and sum of squares due to error (SSE), respectively. Arrows indicate the indices of best fitted models. (J-M) represent the WSC control, WSC injury, SCS control and SCS injury, respectively.

## Results

### *CAP Pattern in WSC and SCS Preparations*

Mono and biphasic peaks were detected in recorded CAPs based on the stimulus intensity and electrode distance (Fig. 2-A, B). The appropriate setting of conduction length in spinal cord made it possible to monitor the activities of slower fibers with CVs of less than 8 m/s.

SCS preparations showed a biphasic peak in most of the records. The second wave in SCS records showed the same CV properties of non-myelinated WM known as "C-wave" (Fig. 2-A). Even at the expense of high stimulus intensities (1-3 V, 0.1 ms peak to peak) no high amplitude peak was monitored in WSC preparations. However, there was a high amplitude CAP recorded in SCS preparation even at the expense of moderate stimulus intensity (0.8-1 V, 0.1 ms peak to peak). The WSC excitability was achieved at higher threshold than SCS (Fig. 2-A, B).

### *Corresponding Pathways in WSC and SCS Preparations*

There was a combination of pyramidal and extra-pyramidal pathways acting in all of WSC and SCS preparations. Both of these pathways are part of descending motor pathways (efferent) (Fig. 1 A-C). Rubrospinal, reticulospinal and olivospinal tracts of extrapyramidal pathway showed to be vulnerable to damage through SCS preparation (Fig. 1-B). Regarding this point, SCS CAP of intact spinal cord mostly represented the CV of lateral corticospinal (LCS) and anterior corticospinal (ACS) tracts of pyramidal pathway in combination with the vestibulospinal tract of extrapyramidal pathway. Distribution of spinal cord conductive pathways and "C bouton" neuromodulators are shown schematically (Fig. 1 A-C). "C boutons" were also highly damaged through preparation of longitudinal strips due to their proximity to medial cutting edge (Fig. 1-B).

### *Effect of Abrupt Compression on the Amplitude, Latency and Conduction of SCS and WSC Preparations*

Introduction of Aneurism clip at T13 level imposed about 60 kpa pressure on WSC and SCS preparations. This amount of pressure caused a highly significant decline in WSC CAP amplitude (42.33% of its control state, p-value<0.0001). There was also a highly significant decline in the amplitude of SCS CAP waves caused by the same procedure. The CAP amplitude of the first and second waves declined up to 58.65% and 12.47% of the control state (p-values<0.0001), respectively. However, there was more vulnerability toward amplitude decline in SCS rather WSC records.

Latency of both monophasic WSC and biphasic SCS increased significantly So that there was a 143.24% increase in peak latency in monophasic WSC against control (p-value<0.0001). There was also a 115.58% and 197.39% increase in the latency of the first and second SCS waves in comparison to control (p-values<0.0001). In other words, SCS second wave showed more increase in latency in comparison to the first wave (Fig. 2-D).

As mentioned above, fiber conduction was measured from total area under curve using Simpson method. Fibers conduction declined significantly in both WSC and SCS CAPs following compression. There was a 61.37% and 11.51% decline in fiber conduction respect to control (p-values<0.0001) (Fig. 2-E).

### *CVs of WSC and SCS Preparations*

Conduction velocity of WSC was 38.46 ± 1.6 m/s. The fastest and the slowest CVs of SCS were 15 ± 0.8 and 4.5 ± 0.18 m/s, respectively. It was revealed that at the expense of similar stimulation, more uniform fast fibers were recruited in the control WSC than SCS. There were also thicker myelinated fibers involved in the formation of WSC than SCS CAPs (Fig 2-A, B, D).

### *Representation of WSC and SCS Compression in Fitted Equations*

Application of goodness of fitting evaluation indices approved the appropriateness of Gaussian model as the best curve fitting model. The best level of proposed Gaussian model for each state describes the CAPs characteristics inclusively (Table 1).

In cases where the adjusted R2, SSE and RMSE of model levels were the same, the prediction bound worked out the level of fitting model (Fig. 3-Step3). The goodness of fitting indices in WSC CAP control in G4 (Gaussian level 4) were inferior in contrast to G5 (Fig. 3-Step3 J-1, 2). However, G4 was as approved to be the best fit due to its better prediction bounds (Fig. 3-Step2 H, I).

The abrupt compression caused a drop in the level of fitting model in both WSC and SCS preparations. The WSC control state was best fitted using Gaussian model 4 "G4" (Fig. 3-step 3 J1-2). The model level fell into G3 after compression (Fig. 3, step K1-2; Table 1). There was a similar scenario occurred in SCS compression.

**Table 1.** Recommended fitting models for each stage of injury. 'G' stands for Gaussian model and its corresponding number clarifies the level of fitting model. Calculated adjusted $R^2$, (RMSE) Root Mean Squared Error and (SSE) Sum of Squares due to Error are shown for each of the fitting models

| Type of preparation | Treatment groups | Gaussian fitting model | Goodness of fitting evaluation parameters | Terms of the fitted model equation |
|---|---|---|---|---|
| Whole Spinal cord (WSC) | *Control* | G 4 | SSE:34.8, $R^2$:0.9983, Adjusted-$R^2$:0.9983, RMSE:0.2301 | y = 69.63.*exp(-((x-0.1169)/ 0.0876).^2) + 31.34.*exp(-((x-0.8127)/ 1.402).^2) + 85.36.*exp(-((x+0.104)/ 4.142).^2) - 9.232e+013.*exp(-((x+166.5)/ 31.88).^2) |
| | *Contusion* | G 3 | SSE:126.6, $R^2$:0.9704, Adjusted-$R^2$:0.9701, RMSE:0.4443 | y =52.88.*exp(-((x-0.1722)/0.2804).^2) + 6.531.*exp(-((x-4.144)/5.766).^2) - 7.606 .*exp(-((x-0.8167)/1.368).^2) |
| Spinal cord strips (SCS) | *Control* | G 6 | SSE:370.3, $R^2$:0.9937, Adjusted-$R^2$:0.9936, RMSE:0.763 | y = -35.43.*exp(-((x-0.9891)/0.4186).^2) + 12.74.*exp(-((x-2.264)/0.4721).^2) + 23.24.*exp(-((x-3.949)/1.182).^2) + 5.454.*exp(-((x-5.813)/1.034).^2) + 9.71.*exp(-((x-11.05)/2.386).^2) + 15.25.*exp(-((x-2.891)/0.7223).^2) |
| | *Contusion* | G 3 | SSE:106.8, $R^2$:0.9842, Adjusted-$R^2$:0.984, RMSE:0.4088 | y = -1.924e+005.*exp(-((x-1.018)/0.2912).^2) + -1.924e+005.*exp(-((x-1.018)/0.2912).^2) + 12.43.*exp(-((x-1.394)/2.347).^2) |

Gaussian model 6 "G6" was found to be the best fit for SCS intact CAP that fell into three levels lower "G3" due to the implemented compression (Fig. 3, step L1-2 and M1-2; Table 1).

## Discussion

The patterns of CAP in WSC and SCS are different at certain similar distant positions of stimulating and recording electrodes. There would be a properly reproducible second peak appearing in SCS CAPs at certain (40-45 mm) distance [5]. The recorded CAP of WSC in the double sucrose gap apparatus was mostly monophasic. The complexity of the SCS control CAP pattern was manifested based on curve fitting model level showing two degrees more than WSC best fitted model (Table 1). This fact reveals that more heterogeneous fibers with different level of myelination and CV are recruited in SCS preparation than WSC ones. Both WSC and SCS preparations represented the same fitting model level (G3) after receiving severe abrupt compression (Table 1). This point implies that all recruited fibers in CAPs were highly damaged through contusion. In other words, level three of Gaussian fitting model (G3) demonstrated the death phase of spinal cord cells in both SCS and WSC preparations.

Myelination is highly correlated with conduction velocity (CV) and latency of CAP peaks whether in intra-axonal or field potential stimulated records [15]. The demyelinated axons exhibit reduced CV and lower ability of conduction following high frequency stimulation. This phenomenon is monitored by the increase in peak latency [16, 17]. The MNs are known as the most highly myelinated fibers in spinal cord. thus, changes in CAP peak latency is the most interrelated factor that addresses myelin loss and MNs damage [5]. Reduction in CV and peak latency increment was interpreted as the centroid factor in Gaussian model that represented as "b" in corresponding terms (Equation 2). Overall increment of "b" coefficient represented peak latency increment and MNs demyelination after injury in fitted recorded CAPs (Table 1).

Our result showed the occurrence probability of biphasic WSC CAP as a signature for recurrence of severe damages or attached appendices caused following the excision. WSC provides a monophasic peak on condition that it was extracted intact and all of appendices roots were removed unconditionally [2]. Considering the corresponding fibers in biphasic CAPs, there would be two justifications; first, the interference of attached fibers including Remak bundles would be the reason for the WSC biphasic CAP appearance and second, the probable damage to the grey matter including "C boutons" would disrupt the low threshold hyperpolarization of MNs. This led to the loss of synchronized excitation of WSC recorded CAPs presented as biphasic CAP. Considering the lower probability of damage to the grey matter of spinal cord excised from vertebral column, the former reason seems more plausible.

The larger diameter of axons is concurrent to the faster CVs [18]. The WSC CAP excitation threshold showed higher speed than SCS but fibers with higher CVs seemed to have been recruited (38.46 m/s against 15 m/s CV of SCS fast fibers). In other word, more low-myelinated fibers were recruited in SCS CAP in comparison to WSC CAP. Antidromic CV of the corticospinal tract in rat has been studied though monopolar stimulation (0.75-1.25 mA) and reported to be about 3-11 m/s [19]. Consequently, the CV of first and second CAP peaks in SCS preparation are in the range of pyramidal pathway corticospinal tract. This also confirms the extrapyramidal destruction caused by SCS preparation. On the other hand, reticulospinal tract of extrapyramidal pathway showed a CV of about 16-80 m/s (mean = 37 m/s) that was very close to the CV of WSC CAP single peak [19]. The fastest and the slowest CVs of SCS identified here were very close to reported CVs matching the speed in the fast and slow fibers with diameters ranging from 4.8 to 6.5 µm, respectively [5].

Higher MN excitability occurred in SCS than in WSC preparations due to larger amplitude gained in response to lower stimulus (Fig. 1 A-C, Fig. 2). It is on condition that the relative loss of extrapyramidal impact that is equal to the loss of high CV fibers recruit is more considerable in SCS control CAP than in WSC. This controversy is concurrent to higher “C boutons” loss in SCS preparation. It was expected to have less SCS excitability when “C boutons” that are proximal to central canal, were highly damaged during longitudinal strip preparation. However, not only the extrapyramidal injury and “C boutons” loss in SCS preparation did not diminish but reinforced it. Thus it is concluded that the MN signals mostly pass through pyramidal pathway either in ventral or dorsal longitudinal strips in SCS preparations. Our results imply that an increased excitability occurred in less myelinated fibers at the expense of regulated excitability loss in highly myelinated fibers. This compensatory trend leads to overall increased excitability in SCS rather WSC preparation. Our proposed mechanism might be applied to describe the dysreflexia and episodic hypertention occurring in mammals following spinal cord injury (SCI) due to the superseded pathways recruited [20].

In brief, WSC CAP represented the involved tracts and fibers of extrapyramidal pathway while SCS CAP peaks manifest pyramidal pathway function exclusively. Here, we aimed to introduce an inclusive monitoring system to provide reproducible CAP in both isolated WSC and SCS preparations. Thus, changes in monophasic and biphasic recorded CAPs were monitored according to the Gaussian model using Trust-region algorithm. It was also aimed to interpret the CAP waves based on the corresponding tracts and fibers to address the activity of individual fibers involved in CAP produced in isolated spinal cord.

The outcome of the approach taken here will shed further light on the application of real time electrophysiological in practical research approaches. This approach also tries to address the integrity and activity of involved fibers and their ultimate physiological function in a more precise manner.

## Acknowledgements

The financial support of the University of Tehran is greatly appreciated.

## References

1. Zeilhofer, H. U., Wildner, H., and Yévenes, G. E. Fast synaptic inhibition in spinal sensory processing and pain control. Physiological reviews, **92**(1): 193-235 (2012).
2. Velumian A.A. ,Wan Y. ,Samoilova M., and Fehlings M.G. Modular double sucrose gap apparatus for improved recording of compound action potentials from rat and mouse spinal cord white matter preparations. J. Neurosci. Methods, **187**(1): 33-40 (2010).
3. Eftekharpour E. ,Karimi-Abdolrezaee S. ,Sinha K. ,Velumian A.A. ,Kwiecien J.M., and Fehlings M.G. Structural and functional alterations of spinal cord axons in adult Long Evans Shaker (LES) dysmyelinated rats. Exp. Neurol., **193**(2): 334-349 (2005).
4. Goryawala M. ,Yaylali I. ,Cabrerizo M. ,Vedala K., and Adjouadi M. An effective intra-operative neurophysiological monitoring scheme for aneurysm clipping and spinal fusion surgeries. J. Neural. Eng., **9**(2): 026021 (2012).
5. Velumian A.A. ,Wan Y. ,Samoilova M., and Fehlings M.G. Contribution of fast and slow conducting myelinated axons to single-peak compound action potentials in rat spinal cord white matter preparations. J. Neurophysiol., **105**(2): 929-941 (2011).
6. Dimitrijevic M.R. ,Kakulas B.A. ,McKay W.B., and Vrbova G. Restorative neurology of spinal cord injury. OUP USA, (2012).
7. Murinson B.B., and Griffin J.W. C-fiber structure varies with location in peripheral nerve. J Neuropathol Exp. Neurol., **63**(3): 246-254 (2004).
8. Moalem-Taylor G. ,Lang P.M. ,Tracey D.J., and Grafe P. Post-spike excitability indicates changes in membrane potential of isolated C-fibers. Muscle Nerve, **36**(2): 172-182 (2007).
9. Miles G.B. ,Hartley R. ,Todd A.J., and Brownstone R.M. Spinal cholinergic interneurons regulate the excitability of motoneurons during locomotion. Proc. Natl. Acad. Sci. U S A, **104**(7): 2448-2453 (2007).
10. Shi R., and Borgens R.B. Anatomical repair of nerve membranes in crushed mammalian spinal cord with polyethylene glycol. J. Neurocytol., **29**(9): 633-643 (2000).

11. MathWorks I. Curve fitting toolbox: for use with MATLAB®: user's guide. MathWorks, (2002).
12. Ondrejcak T. ,Vanicky I. ,Galik J., and Saganova K. Chronically implanted electrodes for repeated stimulation and recording of spinal cord potentials. J. Neurosci. Methods., **141**(1): 125-134 (2005).
13. Pryor J., and Shi R. Electrophysiological changes in isolated spinal cord white matter in response to oxygen deprivation. Spinal Cord, 44(11): 653-661 (2006).
14. Liengme B.V. A guide to Microsoft Excel 2007 for scientists and engineers. Academic Press, (2009).
15. Kohama I. ,Lankford K.L. ,Preiningerova J. ,White F.A. ,Vollmer T.L., and Kocsis J.D. Transplantation of cryopreserved adult human Schwann cells enhances axonal conduction in demyelinated spinal cord. J. Neurosci., **21**(3): 944-950 (2001).
16. Honmou O. ,Felts P.A. ,Waxman S.G., and Kocsis J.D. Restoration of normal conduction properties in demyelinated spinal cord axons in the adult rat by transplantation of exogenous Schwann cells. J. Neurosci., **16**(10): 3199-3208 (1996).
17. Nashmi R., and Fehlings M.G. Mechanisms of axonal dysfunction after spinal cord injury: with an emphasis on the role of voltage-gated potassium channels. Brain Res. Brain Res. Rev., **38**(1-2): 165-191 (2001).
18. Jensen J.M., and Shi R. Effects of 4-aminopyridine on stretched mammalian spinal cord: the role of potassium channels in axonal conduction. J. Neurophysiol., **90**(4): 2334-2340 (2003).
19. Kalderon N., and Fuks Z. Severed corticospinal axons recover electrophysiologic control of muscle activity after x-ray therapy in lesioned adult spinal cord. Proc. Natl. Acad. Sci. U S A, **93**(20): 11185-11190 (1996).
20. Krassioukov A.V., and Weaver L.C. Reflex and morphological changes in spinal preganglionic neurons after cord injury in rats. Clin. Exp. Hypertens, **17**(1-2): 361-373 (1995).